Electron gyroscale fluctuation measurements in National Spherical Torus Experiment H-mode plasmas[a)]

D. R. Smith,[1,b)] S. M. Kaye,[1] W. Lee,[2] E. Mazzucato,[1] H. K. Park,[2] R. E. Bell,[1] C. W. Domier,[3] B. P. LeBlanc,[1] F. M. Levinton,[4] N. C. Luhmann, Jr.,[3] J. E. Menard,[1] and H. Yuh[4]

[1]*Princeton Plasma Physics Laboratory, Princeton, New Jersey 08543, USA*
[2]*Pohang University of Science and Technology, Pohang 790-784, Korea*
[3]*Department of Applied Science, University of California at Davis, Davis, California 95616, USA*
[4]*Nova Photonics, Inc., Princeton, New Jersey 08540, USA*

(Received 3 August 2009; accepted 20 October 2009; published online 11 November 2009)

A collective scattering system has measured electron gyroscale fluctuations in National Spherical Torus Experiment [M. Ono *et al.*, Nucl. Fusion **40**, 557 (2000)] H-mode plasmas to investigate electron temperature gradient (ETG) turbulence. Observations and results pertaining to fluctuation measurements in ETG-stable regimes, the toroidal field scaling of fluctuation amplitudes, the relation between fluctuation amplitudes and transport quantities, and fluctuation magnitudes and k-spectra are presented. Collectively, the measurements provide insight and guidance for understanding ETG turbulence and anomalous electron thermal transport. © *2009 American Institute of Physics*. [doi:10.1063/1.3262530]

I. INTRODUCTION

Anomalous electron thermal transport in magnetically confined plasma hinders efforts to achieve feasible magnetic fusion energy. Nonlinear gyrokinetic simulations indicate that electron temperature gradient (ETG) turbulence can generate experimentally relevant electron thermal transport for certain plasma regimes.[1–4] ETG turbulence occurs on the electron gyroscale with $k_\perp \rho_e \lesssim 1$, where $k_\perp$ is the fluctuation wavenumber perpendicular to the magnetic field and ρ_e is the electron gyroradius. Nonlinear gyrokinetic simulations predict that ETG turbulence can saturate at higher normalized amplitude and generate greater normalized transport than ion temperature gradient (ITG) turbulence.[5–7] Secondary instabilities and zonal flows regulate drift wave instabilities, such as the ETG and ITG modes. The ion response for ETG turbulence, however, weakens ETG secondary instabilities in relation to ITG turbulence. To test predictions of ETG turbulence from nonlinear gyrokinetic simulations, fluctuation measurements on the electron gyroscale are needed.

The National Spherical Torus Experiment[8,9] (NSTX) is a low-aspect-ratio tokamak well suited for investigating ETG turbulence and electron thermal transport. NSTX H-mode plasmas with neutral beam injection (NBI) exhibit ion thermal transport at or near neoclassical levels, and electron thermal transport is always anomalous and dominant in most cases. Toroidal rotation from NBI generates large equilibrium $E\times B$ flow shear rates that typically exceed ITG and trapped-electron mode (TEM) growth rates. Neoclassical ion thermal transport in NSTX H-mode plasmas with NBI is attributed to the inferred flow shear suppression of ITG and TEM turbulence. The ETG mode, on the other hand, can be linearly unstable in NSTX plasmas with growth rates exceeding $E\times B$ flow shear rates. Accordingly, NSTX is well suited for investigating ETG turbulence.

To investigate ETG turbulence, a collective scattering system was installed on NSTX to measure electron gyroscale fluctuations.[10–12] The NSTX collective scattering system simultaneously measures up to five distinct wavenumbers with $k_\perp \rho_e \lesssim 0.6$. The scattering system is configured for tangential measurements. Measured wave vectors are primarily radial with $k_\theta / k_r \approx 0.1-0.3$, where k_r is the radial wavenumber and k_θ is the binormal wavenumber such that $k_\theta > 0$ corresponds to the ion drift direction. With heterodyne detection, the scattering system can distinguish modes that propagate with a component in the ion drift directions and modes that propagate with a component in the electron drift direction. The radial localization and k-space resolution are $\Delta R \approx \pm 3$ cm and $\Delta k_\perp \approx 1$ cm^{-1}, respectively, and steerable optics can position the scattering volume from the magnetic axis to the last-closed flux surface.

Past collective scattering measurements in NSTX revealed electron gyroscale fluctuations in L-mode plasmas with high-harmonic fast-wave heating.[13,14] Enhanced fluctuations were observed when the local ETG exceeded the ETG linear critical gradient, and the enhanced fluctuations propagated with a component in the electron diamagnetic direction. In H-mode plasmas with NBI heating, scattering measurements revealed electron gyroscale fluctuations when the ETG was marginally stable with respect to the ETG linear critical gradient, and fluctuation amplitudes decreased when the equilibrium $E\times B$ shear rate exceeded ETG linear growth rates.[15] In this paper, we investigate several additional topics including fluctuation measurements in ETG-stable regimes in Sec. II, the toroidal field scaling of fluctuation amplitudes in Sec. III, the relationship between

[a)]Based on an invited talk given at the 2008 APS DPP Meeting in Dallas, Texas. Paper YI2 5, Bull. Am. Phys. Soc. **53**, 323 (2008).
[b)]Invited speaker. Electronic mail: drsmith@pppl.gov. Present address: Department of Engineering Physics, University of Wisconsin-Madison, Madison, WI 53706, USA.

 © 2009 American Institute of Physics

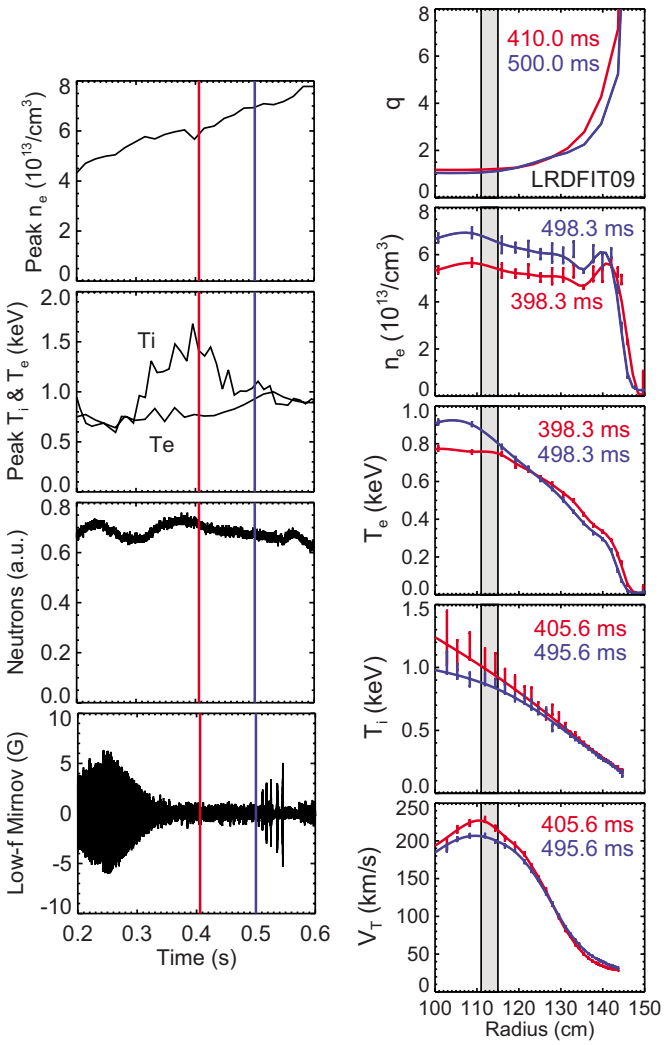

FIG. 1. (Color online) Discharge 124887 with deuterium gas, B_T=4.5 kG, I_p=700 kA, and 4 MW of NBI heating. Fluctuation measurements were obtained at $R=113\pm2$ cm (gray box).

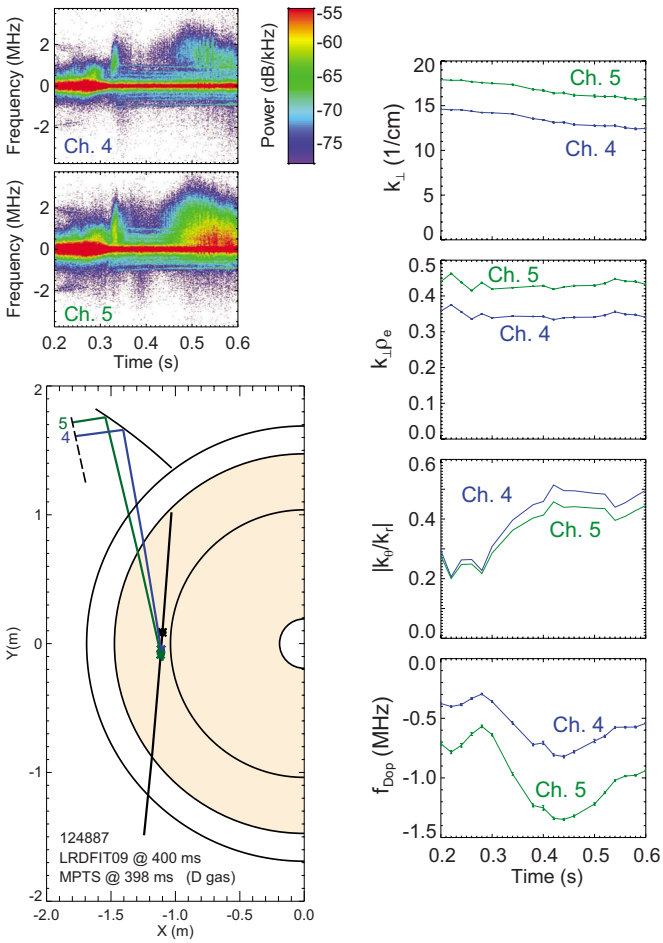

FIG. 2. (Color online) Fluctuation measurements and ray tracing calculations for discharge 124887 at $R=113\pm2$ cm in Fig. 1.

fluctuation amplitudes and transport quantities in Sec. IV, and fluctuation magnitudes and k-spectra in Sec. V.[16] Finally, Sec. VI presents a summary of results.

II. FLUCTUATION MEASUREMENTS IN ETG-STABLE REGIONS

This section presents electron gyroscale fluctuation measurements in H-mode discharges near the magnetic axis where the ETG is small.[16] Electron gyroscale fluctuations associated with ETG turbulence should not be observed if the ETG is less than the ETG critical gradient. Additionally, the region near the magnetic axis in H-mode plasmas ($r/a\lesssim0.2$) exhibits small equilibrium $E\times B$ shear rates, similar to the L-mode plasmas with high harmonic fast wave (HHFW) heating in Refs. 13 and 14.

Figure 1 shows discharge profiles for a 4.5 kG H-mode plasma with fluctuation measurements at $R=113\pm2$ cm and $r/a=0.1-0.2$. The Mirnov signal is approximately steady state for the period 340–500 ms, and the neutron signal does not show fast-ion loss events. Note that the $E\times B$ shear rate is relatively low at about 20–30 kHz. Figure 2 shows fluctuation measurements and ray tracing calculations at $R=113\pm2$ cm and $r/a=0.1-0.2$. Enhanced fluctuations occur briefly at 330 ms and persist after 450 ms. In Fig. 2, positive frequency corresponds to fluctuations that propagate with a wave vector component in the ion drift direction in the *laboratory* frame. Toroidal rotation induces a Doppler shift toward the ion direction such that peak amplitudes in Fig. 2 correspond to fluctuations that propagate with a wave vector component in the electron drift direction in the *plasma* frame. Accordingly, the wavenumber range and propagation direction of the measured fluctuations in Fig. 2 are consistent with ETG turbulence. Note that ray tracing calculations indicate that the length of the scattering volume along the probe beam in Fig. 2 is less than 1 cm. The nearly toroidal magnetic field near the magnetic axis generates the narrow selectivity function.[17,18] The peak in the instrument selectivity function, however, varies by about 3 cm along the probe beam for rays within the probe beam antenna pattern. A realistic calculation of the scattering volume length near the magnetic axis may require a full-wave calculation. In addition, spectral features in the range of 1–2 MHz in Fig. 2 are consistent with Doppler-shifted fluctuations with calculated toroidal wavenumbers, so the observed fluctuations are consistent with high-k fluctuations.

Figure 3 shows ETG critical gradients and growth rates

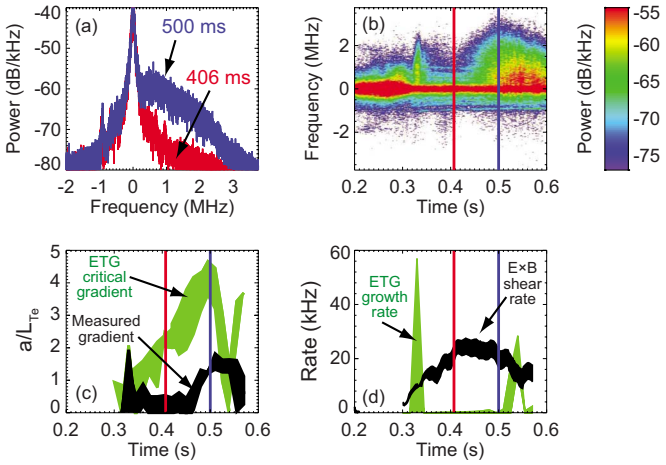

FIG. 3. (Color online) [(a) and (b)] Fluctuation measurements for Sec. V, (c) ETG and ETG linear critical gradient, and (d) $E\times B$ shear rate and ETG linear growth rate for data in Figs. 1 and 2.

from GS2 linear gyrokinetic calculations for measurements in Figs. 1 and 2. GS2 is an initial value, continuum gyrokinetic code, and fully electromagnetic.[5,6] The GS2 calculations include eight modes in the range $5<k_\theta\rho_s<25$, where ρ_s is the ion sound radius. The ETG is varied in GS2 calculations to find the ETG critical gradient at which growth rates vanish. The brief period of enhanced fluctuations at 330 ms occurs when the ETG briefly exceeds the ETG critical gradient. The increase in fluctuation amplitudes after 450 ms, however, occurs during a period of ETG stability. The measurements indicate that electron gyroscale fluctuations are present during a period of ETG linear stability. The observations are inconsistent with linear stability theory for ETG turbulence and suggest that an additional turbulence mechanism is present, possibly high-k microtearing modes. Alternatively, the observed fluctuations may be a high-k cascade generated by low-k ITG/TEM turbulence.[2] At the measurement location near the core, the $E\times B$ shear is about 20 kHz compared to about 100 kHz at midradii, so $E\times B$ shear may be insufficient to suppress low-k turbulence near the core.

Figure 4 shows discharge profiles for a 5.5 kG H-mode plasma with fluctuation measurements at $R=113\pm2$ cm and $r/a=0.1-0.2$. The low frequency Mirnov signal is steady state after 400 ms, and the neutron signal indicates that fast-ion losses are absent. Figure 5 shows fluctuation measurements and ray tracing calculations at $R=113\pm2$ cm and $r/a=0.1-0.2$. Enhanced fluctuations occur between 400 and 450 ms and after 600 ms. In Fig. 5, positive frequency corresponds to fluctuations that propagate with a wave vector component in the ion drift direction in the *laboratory* frame. Toroidal rotation induces a Doppler shift toward the ion direction such that peak amplitudes in Fig. 5 correspond to fluctuations that propagate with a wave vector component in the electron drift direction in the *plasma* frame. Accordingly, the wavenumber range and propagation direction of the observed fluctuations are consistent with ETG turbulence. As in Fig. 2, the scattering volume length along the probe beam in Fig. 5 is less than 1 cm. However, the peak in the selectivity

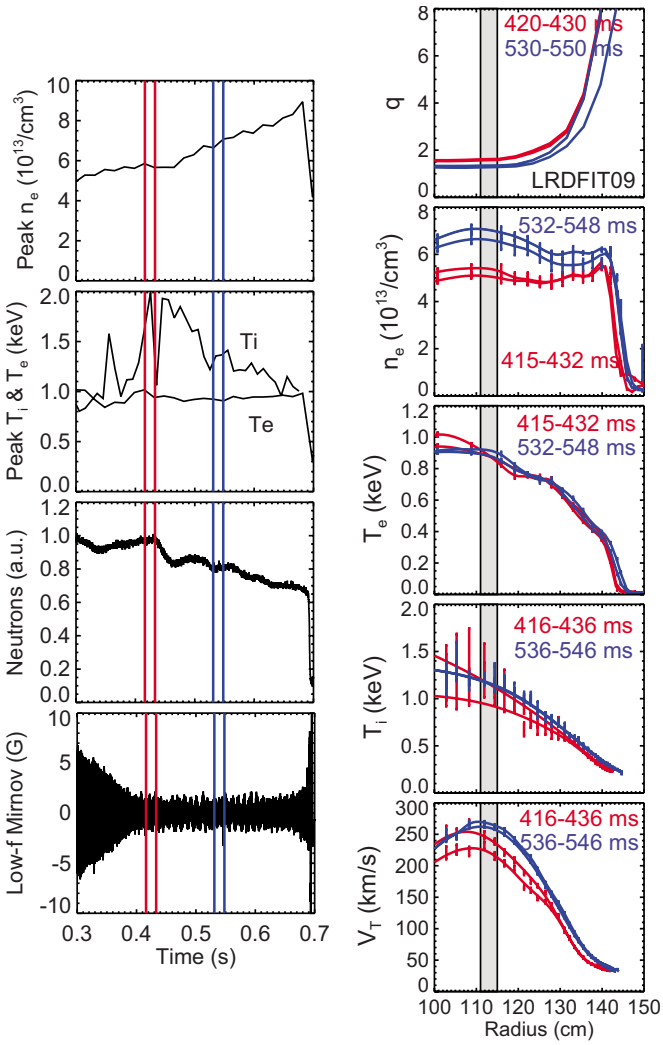

FIG. 4. (Color online) Discharge 124885 with deuterium gas, $B_T=5.5$ kG, $I_p=700$ kA, and 4 MW of NBI heating. Fluctuation measurements were obtained at $R=113\pm2$ cm (gray box).

function varies by about 3 cm along the probe beam for rays within the probe beam antenna pattern, and the observed fluctuations are consistent with Doppler-shifted high-k fluctuations. Figure 6 shows ETG critical gradients for data in Figs. 4 and 5. Figure 6 does not show ETG growth rates because ETG modes are linearly stable for the entire time period due to the flat electron temperature profile. The measurements indicate that electron gyroscale fluctuations are present during a period of ETG linear stability. Again, the observations are inconsistent with linear stability theory for ETG turbulence and suggest that an additional turbulence mechanism is present.

III. TOROIDAL FIELD SCALING OF FLUCTUATION AMPLITUDES

H-mode confinement studies on NSTX indicate that confinement improves at higher B_T largely due to reduced χ_e in the outer plasma, $r/a\gtrsim0.5$.[19,20] The NSTX confinement time scaling for B_T is stronger than conventional tokamak scalings. Specifically, the NSTX energy confinement time scaling is $\tau_E\sim B_T^{0.85}$, but the ITER98PB,2 scaling is $\tau_E\sim B_T^{0.15}$. To

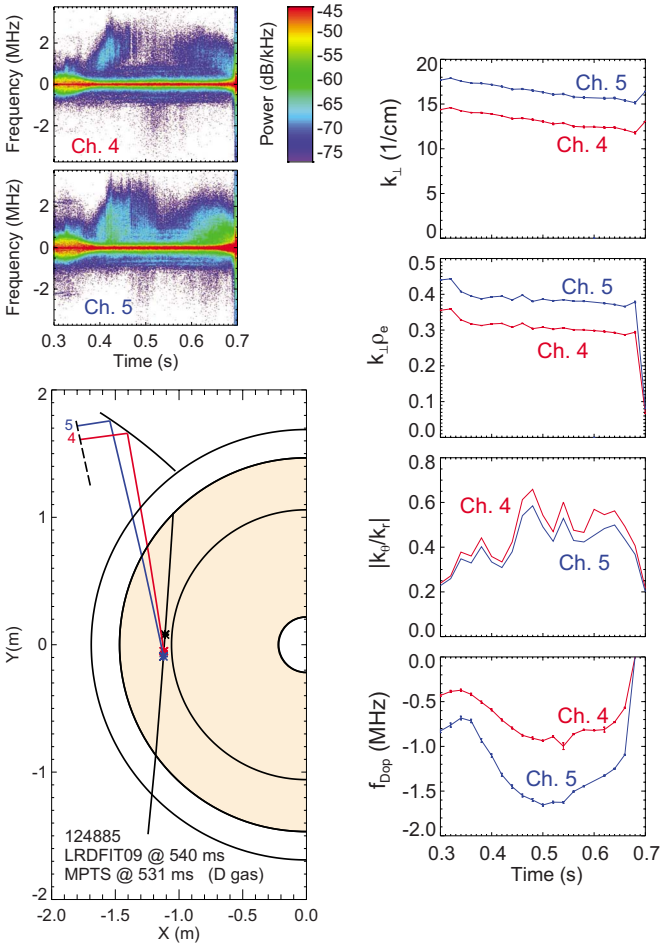

FIG. 5. (Color online) Fluctuation measurements and ray tracing calculations for discharge 124885 at $R=113\pm2$ cm in Fig. 4.

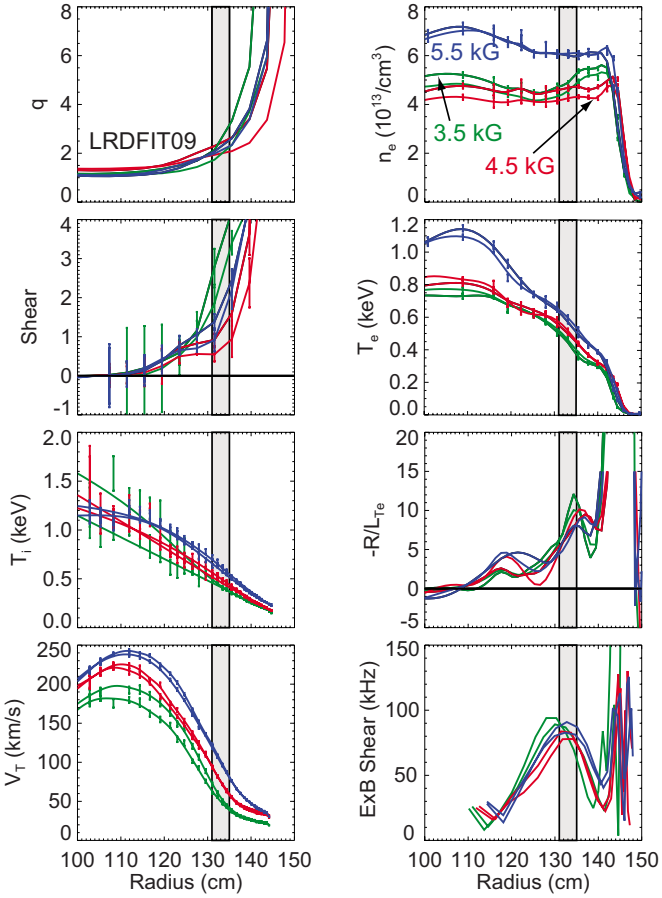

FIG. 7. (Color online) Discharge profiles for multiple discharges at $R=133\pm2$ cm. The gray box marks the location of fluctuation measurements: 124892 with $B_T=3.5$ kG at 340 ms, 124888 with $B_T=4.5$ kG at 350 ms, and 124889 with $B_T=5.5$ kG at 600 ms.

investigate the B_T scaling of electron gyroscale fluctuations, fluctuation measurements were obtained for H-mode discharges with 3.5, 4.5, and 5.5 kG toroidal fields.[16]

Figure 7 shows profile quantities for 3.5, 4.5, and 5.5 kG discharges, and Fig. 8 shows $E\times B$ shear rates, ETG linear growth rates, and fluctuation measurements. Discharge times were selected to best match ETGs, $E\times B$ shear rates, and

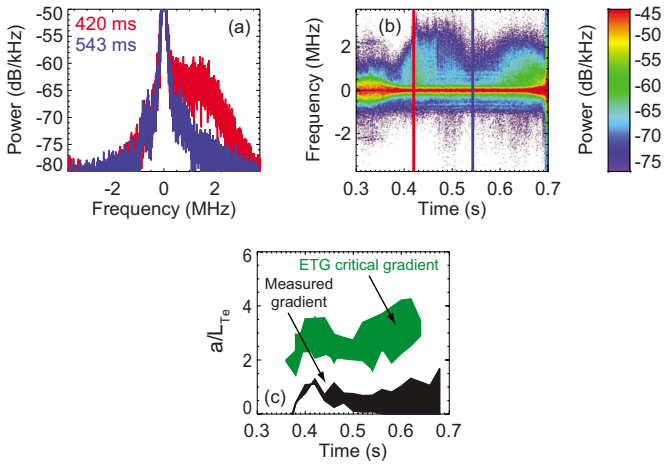

FIG. 6. (Color online) [(a) and (b)] Fluctuation measurements for Sec. V and (c) ETG and ETG linear critical gradient for data in Figs. 4 and 5.

ETG linear growth rates. Fluctuation amplitudes for the 3.5 kG discharge exceed amplitudes in the 4.5 kG discharge by more than 10 dB, but amplitudes in the 4.5 kG discharge are only about 5 dB greater than amplitudes in the 5.5 kG discharge. Note that $E\times B$ shear rates and ETG growth rates are similar for the 3.5 and 5.5 kG discharges, but the 4.5 kG discharge exhibits $E\times B$ shear rates noticeably greater than ETG growth rates. Accordingly, fluctuation amplitudes for the 4.5 kG discharge are expected to be disproportionately lower, as observed. Therefore, the measurements indicate that fluctuation amplitudes decrease at higher B_T for similar plasma conditions. Note that the discharges in Figs. 7 and 8 do not exhibit as strong a B_T dependence on confinement as the discharges in Refs. 19 and 20.

IV. FLUCTUATIONS AND TRANSPORT

Feedback mechanisms complicate the relationship between fluctuations amplitudes and transport quantities. For example, if transport diffusivities increase and gradients decrease when fluctuation amplitudes increase, then the inference is that fluctuations induce transport. On the other hand, if fluctuation amplitudes increase when transport diffusivities decrease and gradients increase, then the inference is that fluctuations react to plasma conditions without inducing

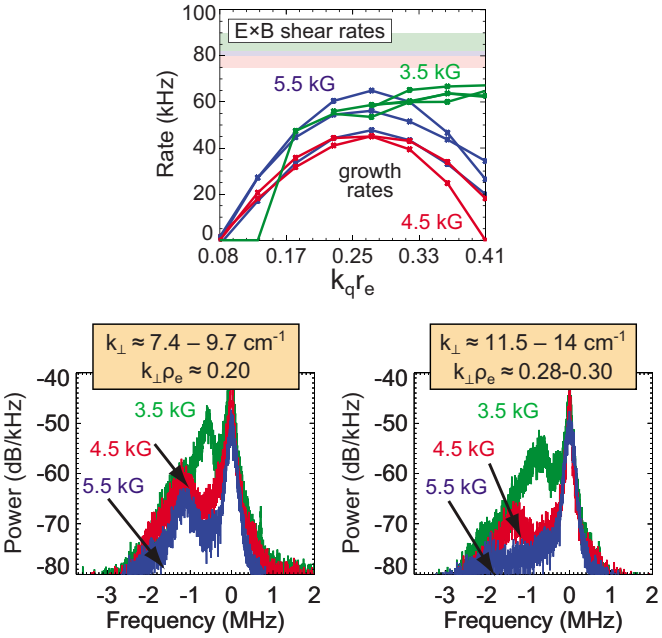

FIG. 8. (Color online) $E \times B$ shear rates, ETG growth rates, and fluctuation measurements for data in Fig. 7: 124892 with B_T=3.5 kG at 340 ms, 124888 with B_T=4.5 kG at 350 ms, and 124889 with B_T=5.5 kG at 600 ms.

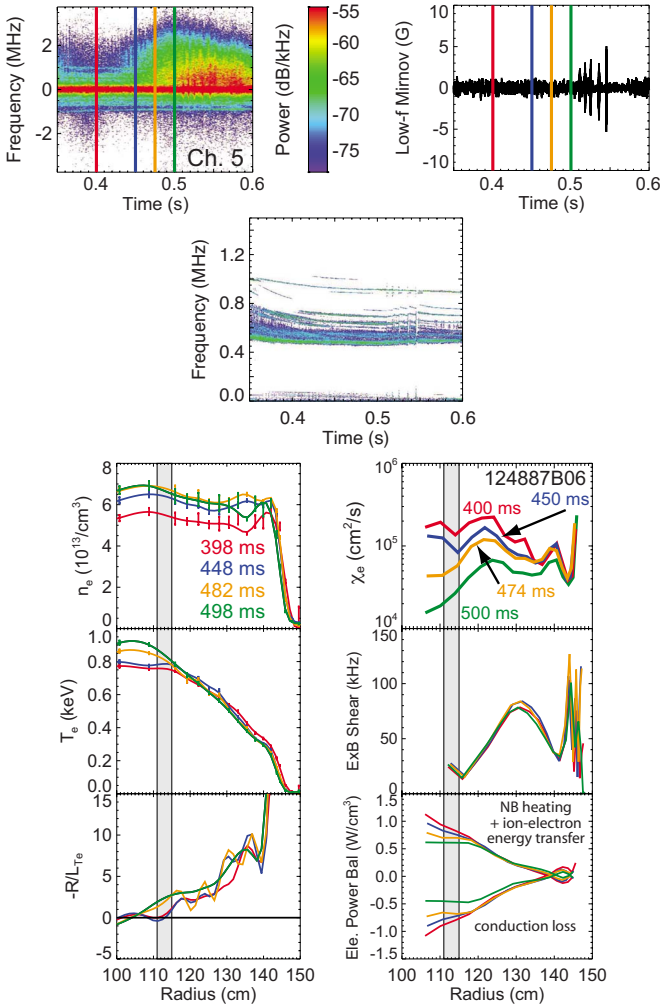

FIG. 9. (Color online) Fluctuation measurements and transport calculations for discharge 124887 at $R=113\pm2$ cm and $r/a\approx0.15$.

transport. Additionally, the relationship between turbulence and transport may depend critically on the phase relation between fluctuations, marginal stability dynamics, or fluctuation correlation lengths. This section presents fluctuation measurements and TRANSP calculations[21,22] to investigate the relationship between electron gyroscale fluctuation amplitudes and electron thermal transport.[16]

Figure 9 shows fluctuation measurements and transport calculations at $R=113\pm2$ cm and $r/a\approx0.15$ for discharge 124887, a 4.5 kG H-mode discharge (see Fig. 1). Recently, Global Alfven eigenmodes (GAEs) were proposed as a mechanism for anomalous electron thermal transport,[23] so it is necessary to monitor GAE activity in Mirnov signals in the range of 0.2–2 MHz. Figure 9 shows that GAE activity is steady state for 400–550 ms, so GAEs apparently cannot account for changes in transport. Measured density fluctuation amplitudes and the local temperature gradient increase from 400 to 550 ms. At the same time, the electron thermal diffusivity and electron heat conduction decrease. The observations suggest that no simple relation exists between measured density fluctuation amplitudes and electron thermal transport. Note that a definitive assessment of the relationship between electron gyroscale fluctuations and electron thermal transport requires simultaneous electric potential and temperature fluctuation measurements.

Figure 10 shows fluctuation measurements and transport calculations at $R=113\pm2$ cm and $r/a\approx0.15$ for discharge 124885, a 5.5 kG H-mode discharge (see Fig. 4). Again, GAE activity is steady state for 550–650 ms, so GAEs apparently cannot account for changes in transport. Fluctuation amplitudes increase from 550 to 650 ms while the temperature gradient remains unchanged. At the same time, the electron thermal diffusivity and electron heat conduction decrease. Again, the observations suggest that no simple relation exists between measured fluctuation amplitudes and electron thermal transport.

V. FLUCTUATION MAGNITUDES AND *k*-SPECTRA

Collective scattering measurements are inherently localized in *k*-space, whereas other fluctuation measurement techniques either employ a spatial array of probes or invoke a theoretical dispersion relation to attain *k*-space information (a notable exception is the Doppler backscattering[24]). Linear gyrokinetic simulations provide linear growth rates and critical gradients, but nonlinear gyrokinetic simulations additionally provide fluctuation magnitudes and *k*-spectra. Fluctuation magnitudes and *k*-spectra from scattering measurements can be valuable validation tests for nonlinear gyrokinetic simulations. Accordingly, this section presents fluctuation magnitudes and *k*-spectra from electron gyroscale fluctuation measurements.[16]

The *k*-space localization of scattering measurements is given by the *k*-matching condition $\boldsymbol{k}_s=\boldsymbol{k}_i\pm\boldsymbol{k}$, where $\boldsymbol{k}_s$ is the scattered wave vector, $\boldsymbol{k}_i$ is the incident wave vector, and $\boldsymbol{k}$ is the measured fluctuation wave vector. The *k*-space resolution is $\Delta k=2/a$. With $k_\parallel\approx0$ ($k_\parallel$ is the component of $\boldsymbol{k}$ parallel to

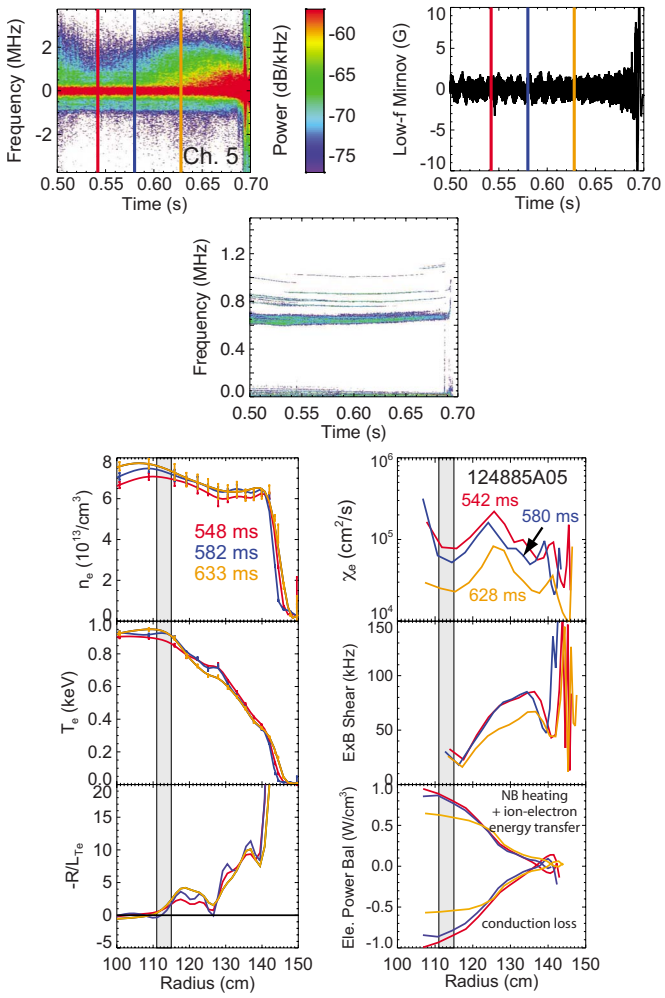

FIG. 10. (Color online) Fluctuation measurements and transport calculations for discharge 124885 at $R=113\pm2$ cm and $r/a\approx0.15$.

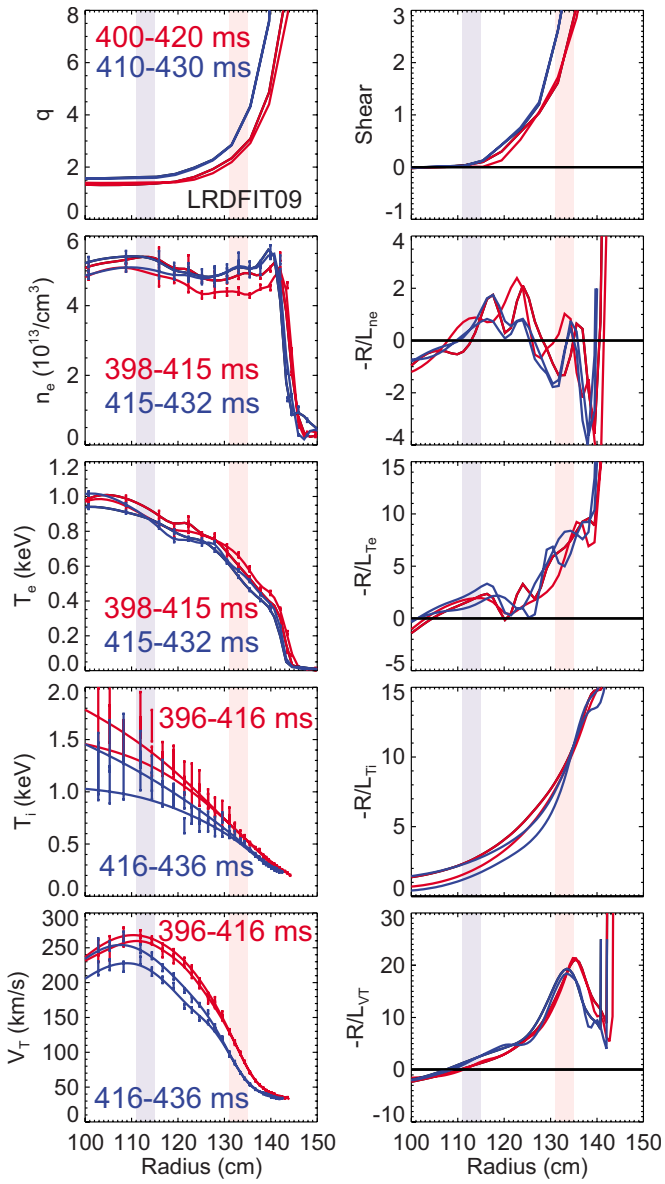

FIG. 11. (Color online) Profile quantities and measurement locations for discharges 124885 at 415–430 ms and 124889 at 400–415 ms.

$\boldsymbol{B}$), scattering measurements are localized to an area $(\Delta k)^2$ in the k_θ-k_r plane. For a coherent density fluctuation with amplitude $\tilde{n}_e$, the total scattered power observed by a receiver with angular aperture $\pi(2/k_i a)^2$ is

$$P_s = \tfrac{1}{4} P_i r_e^2 L_z^2 \lambda_i^2 \tilde{n}_e^2, \tag{1}$$

where λ_i is the probe beam wavelength, $k_i=2\pi/\lambda_i$ is the probe beam wave number, a is the probe beam radius, P_i is the probe beam power, L_z is the length of the scattering volume, and r_e is the classical electron radius. Finally, the wavenumber spectral exponent α is defined such that $|\delta n_e(k)/n_e|^2 \propto k^{-\alpha}$.

Figure 11 shows discharges 124885 and 124889 at times with similar radial profiles. Both discharges have $B_T=5.5$ kG, $I_p=700$ kA, and 4 MW of NBI. Figure 12 shows fluctuation measurements at $R=113\pm2$ cm in 124885 and at $R=133\pm2$ cm in 124889. Multiple detection channels provide k-spectra at both locations. At 133 cm the scattering volume lengths are 3–4 cm. On the other hand, at 113 cm the instrument selectivity function narrows to widths on the order of the probe beam wavelength. The location of the instrument selectivity peak varies by about 3 cm along the probe beam for rays within the probe beam antenna pattern, so the scattering volume length is assumed to be 3 cm. An accurate calculation of the scattering volume for measurement locations near the magnetic axis may require full-wave calculations. In Fig. 12, the spectral exponent at $R=133\pm2$ cm is $\alpha=2.8$, and the spectral exponent at $R=113\pm2$ cm is steeper with $\alpha=4.6$. Additionally, fluctuation magnitudes are in the range $|\delta n_e(k)/n_e|^2\approx10^{-8}$–$10^{-9}$. The vertical error bars correspond to a ±2 dB uncertainty in integrated spectral powers, and the horizontal error bars correspond to the k-space resolution, $\Delta k\approx0.7$ cm^{-1}. Note that fluctuation measurements correspond to a k-space box with area $(\Delta k)^2$, not a k-space annulus in the k_θ-k_r plane. The spectral power uncertainty (±2 dB) corresponds to a spectral exponent uncertainty $\Delta\alpha\approx0.5$.

Nonlinear gyrokinetic simulations in Refs. 2 and 4 predict radial fluctuations magnitudes for typical midradius tokamak parameters. A credible comparison between fluctuation magnitudes in Fig. 12 and Refs. 2 and 4 is not possible

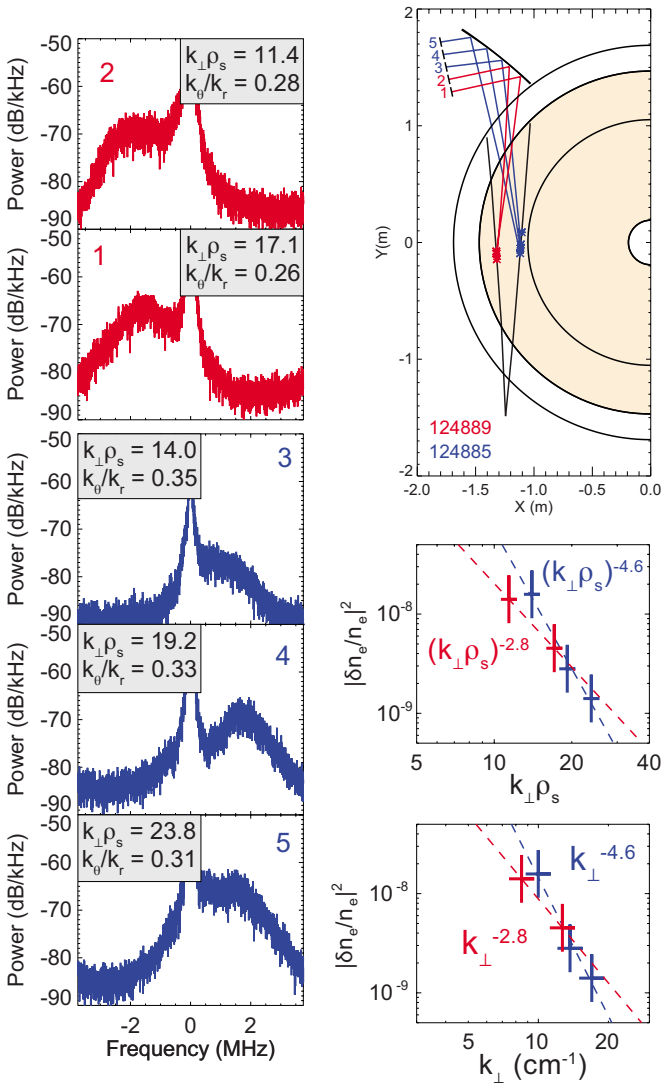

FIG. 12. (Color online) Fluctuation magnitudes and k-spectra for discharges 124885 and 124889 in Fig. 11 are shown.

due to substantial differences between NSTX experimental parameters and simulation parameters, but a cursory comparison is nonetheless informative. Radial fluctuation magnitudes in Ref. 2 are $|\delta n_e/n_e|^2 \approx 10^{-11}-10^{-10}$ for $k_r\rho_s \approx 10-20$ with k-space resolution $\Delta(k_r\rho_s)=0.1$. In Ref. 4, radial fluctuation magnitudes are $|\delta n_e/(n_e\rho_s/R)|^2 \approx 10^{-4}-10^{-2}$ for $k_r\rho_s \approx 10-20$ with k-space resolution $\Delta(k_r\rho_s)=0.1$. With $\rho_s/R \approx 10^{-2}$ for NSTX parameters, fluctuation magnitudes in Ref. 4 are $|\delta n_e/n_e|^2 \approx 10^{-8}-10^{-6}$. Fluctuation magnitudes in Fig. 12 are $|\delta n_e/n_e|^2 \approx 10^{-9}-10^{-8}$, but the k-space resolution is $\Delta(k_\perp\rho_s) \approx 1-2$. If the k-space resolution is converted to $\Delta(k_\perp\rho_s) \approx 0.1$, then fluctuation magnitudes in Fig. 12 can be estimated to be $|\delta n_e/n_e|^2 \approx 10^{-10}-10^{-9}$. Accordingly, fluctuation magnitudes in Fig. 12 are about one order of magnitude larger than fluctuations in Ref. 2 and two to three orders of magnitude smaller than fluctuations in Ref. 4. Approximate agreement in magnitude scales is encouraging but a fully credible comparison is not possible due to substantial differences between NSTX experimental parameters and simulation parameters.

VI. SUMMARY

The NSTX collective scattering system has measured electron gyroscale fluctuations to investigate ETG turbulence. Past measurements revealed electron gyroscale fluctuations in NSTX L-mode plasmas with high-harmonic fast-wave heating.[13,14] Enhanced fluctuations were observed when the local ETG exceeded the ETG linear critical gradient, and the enhanced fluctuations propagated with a component in the electron diamagnetic direction. In NSTX H-mode plasmas with NBI heating, past measurements revealed electron gyroscale fluctuations when the ETG was marginally stable with respect to the ETG linear critical gradient, and fluctuation amplitudes decreased when the equilibrium $E\times B$ shear rate exceeded ETG linear growth rates.[15] This paper has presented observations and results covering several additional topics.[16] Electron gyroscale fluctuations were observed in an ETG-stable region near the magnetic axis in H-mode plasmas. Fluctuation amplitudes decrease at higher toroidal field in plasma regimes with similar ETGs, $E\times B$ shear rates, and ETG linear growth rates. Transport analysis revealed instances in which the electron thermal diffusivity decreased when measured fluctuation amplitudes increased, which suggests that no simple relation exists between measured fluctuation amplitudes and electron thermal transport. Wavenumber spectral exponents are in the range of 2.8–4.6 for H-mode plasmas, and fluctuation magnitudes are $|\delta n_e(k)/n_e|^2 \approx 10^{-9}-10^{-8}$. Finally, fluctuation magnitudes are within one to three orders of magnitude of nonlinear gyrokinetic simulations for midradius tokamak parameters[2,4] when the k-space resolution is taken into account.

ACKNOWLEDGMENTS

This work was supported by the U. S. Department of Energy under Contract Nos. DE-AC02-76CH03073, DE-FG03-95ER54295, and DE-FG03-99ER54518.

[1] W. M. Nevins, J. Candy, S. Cowley, T. Dannert, A. Dimits, W. Dorland, C. Estrada-Mila, G. W. Hammett, F. Jenko, M. J. Pueschel, and D. E. Shumaker, Phys. Plasmas **13**, 122306 (2006).
[2] R. E. Waltz, J. Candy, and M. Fahey, Phys. Plasmas **14**, 056116 (2007).
[3] T. Gorler and F. Jenko, Phys. Rev. Lett. **100**, 185002 (2008).
[4] T. Gorler and F. Jenko, Phys. Plasmas **15**, 102508 (2008).
[5] W. Dorland, F. Jenko, M. Kotschenreuther, and B. N. Rogers, Phys. Rev. Lett. **85**, 5579 (2000).
[6] F. Jenko, W. Dorland, M. Kotschenreuther, and B. N. Rogers, Phys. Plasmas **7**, 1904 (2000).
[7] F. Jenko and W. Dorland, Phys. Rev. Lett. **89**, 225001 (2002).
[8] M. Ono, S. M. Kaye, Y.-K. M. Peng, G. Barnes, W. Blanchard, M. D. Carter, J. Chrzanowski, L. Dudek, R. Ewig, D. Gates, R. E. Hatcher, T. Jarboe, S. C. Jardin, D. Johnson, R. Kaita, M. Kalish, C. E. Kessel, H. W. Kugel, R. Maingi, R. Majeski, J. Manickam, B. McCormack, J. Menard, D. Mueller, B. A. Nelson, B. E. Nelson, C. Neumeyer, G. Oliaro, F. Paoletti, R. Parsells, E. Perry, N. Pomphrey, S. Ramakrishnan, R. Raman, G. Rewoldt, J. Robinson, A. L. Roquemore, P. Ryan, S. Sabbagh, D. Swain, E. J. Synakowski, M. Viola, M. Williams, J. R. Wilson, and NSTX Team, Nucl. Fusion **40**, 557 (2000).
[9] S. M. Kaye, M. G. Bell, R. E. Bell, J. Bialek, T. Bigelow, M. Bitter, P. Bonoli, D. Darrow, P. Efthimion, J. Ferron, E. Fredrickson, D. Gates, L. Grisham, J. Hosea, D. Johnson, R. Kaita, S. Kubota, H. Kugel, B. LeBlanc, R. Maingi, J. Manickam, T. K. Mau, R. J. Maqueda, E. Mazzucato, J. Menard, D. Mueller, B. Nelson, N. Nishino, M. Ono, F. Paoletti, S. Paul, Y.-K. M. Peng, C. K. Phillips, R. Raman, P. Ryan, S. A. Sabbagh, M. Schaffer, C. H. Skinner, D. Stutman, D. Swain, E. Synakowski, Y. Takase, J. Wilgen, J. R. Wilson, W. Zhu, S. Zweben, A.

Bers, M. Carter, B. Deng, C. Domier, E. Doyle, M. Finkenthal, K. Hill, T. Jarboe, S. Jardin, H. Ji, L. Lao, K. C. Lee, N. Luhmann, R. Majeski, S. Medley, H. Park, T. Peebles, R. I. Pinsker, G. Porter, A. Ram, M. Rensink, T. Rognlien, D. Stotler, B. Stratton, G. Taylor, W. Wampler, G. A. Wurden, X. Q. Xu, and L. Zeng, Phys. Plasmas **8**, 1977 (2001).

[10] D. R. Smith, E. Mazzucato, T. Munsat, H. Park, D. Johnson, L. Lin, C. W. Domier, M. Johnson, and N. C. Luhmann, Jr., Rev. Sci. Instrum. **75**, 3840 (2004).

[11] W. Lee, H. K. Park, M. H. Cho, W. Namkung, D. R. Smith, C. W. Domier, and N. C. Luhmann, Jr., Rev. Sci. Instrum. **79**, 10E723 (2008).

[12] D. R. Smith, E. Mazzucato, W. Lee, H. K. Park, C. W. Domier, and N. C. Luhmann, Jr., Rev. Sci. Instrum. **79**, 123501 (2008).

[13] E. Mazzucato, D. R. Smith, R. E. Bell, S. M. Kaye, J. C. Hosea, B. P. LeBlanc, J. R. Wilson, P. M. Ryan, C. W. Domier, N. C. Luhmann, Jr., H. Yuh, W. Lee, and H. Park, Phys. Rev. Lett. **101**, 075001 (2008).

[14] E. Mazzucato, R. E. Bell, S. Ethier, J. C. Hosea, S. M. Kaye, B. P. LeBlanc, W. W. Lee, P. M. Ryan, D. R. Smith, W. X. Wang, J. R. Wilson, and H. Yuh, Nucl. Fusion **49**, 055001 (2009).

[15] D. R. Smith, S. M. Kaye, W. Lee, E. Mazzucato, H. K. Park, R. E. Bell, C. W. Domier, B. P. LeBlanc, F. M. Levinton, N. C. Luhmann, Jr., J. E. Menard, and H. Yuh, Phys. Rev. Lett. **102**, 225005 (2009).

[16] D. R. Smith, Ph.D. dissertation, Princeton University, 2009.

[17] E. Mazzucato, Phys. Plasmas **10**, 753 (2003).

[18] E. Mazzucato, Plasma Phys. Controlled Fusion **48**, 1749 (2006).

[19] S. M. Kaye, F. M. Levinton, D. Stutman, K. Tritz, H. Yuh, M. G. Bell, R. E. Bell, C. W. Domier, D. Gates, W. Horton, J. Kim, B. P. LeBlanc, N. C. Luhmann, Jr., R. Maingi, E. Mazzucato, J. E. Menard, D. Mikkelsen, D. Mueller, H. Park, G. Rewoldt, S. A. Sabbagh, D. R. Smith, and W. Wang, Nucl. Fusion **47**, 499 (2007).

[20] S. M. Kaye, R. E. Bell, D. Gates, B. P. LeBlanc, F. M. Levinton, J. E. Menard, D. Mueller, G. Rewoldt, S. A. Sabbagh, W. Wang, and H. Yuh, Phys. Rev. Lett. **98**, 175002 (2007).

[21] R. J. Goldston, D. C. McCune, H. H. Towner, S. L. Davies, R. J. Hawryluka, and G. L. Schmidt, J. Comput. Phys. **43**, 61 (1981).

[22] R. J. Hawryluk, Proceedings of the Course on Physics of Plasma Close to Thermonuclear Conditions, 1980, Vol. 1, p. 19.

[23] D. Stutman, L. F. Delgado-Aparicio, N. Gorelenkov, M. Finkenthal, E. Fredrickson, S. Kaye, E. Mazzucato, and K. Tritz, Phys. Rev. Lett. **102**, 115002 (2009).

[24] L. Schmitz, G. Wang, J. C. Hillesheim, T. L. Rhodes, W. A. Peebles, A. E. White, L. Zeng, T. A. Carter, and W. Solomon, Rev. Sci. Instrum. **79**, 10F113 (2008).